RECLAMATION

Managing Water in the West

Desalination and Water Purification Research and Development Program Report No. 102

Predicting Membrane Flux Decline Using Parameters Derived from Field-Flow Fractionation Measurements

U.S. Department of the Interior
Bureau of Reclamation

June 2006

REPORT DOCUMENTATION PAGE

Form Approved
OMB No. 0704-0188

1. REPORT DATE *(DD-MM-YYYY)*
June 2006

2. REPORT TYPE
Final

3. DATES COVERED *(From - To)*
Final

4. TITLE AND SUBTITLE
Predicting Membrane Flux Decline Using Parameters Derived from Field-Flow Fractionation Measurements

5a. CONTRACT NUMBER
Agreement No. 01-FC-81-0738

5b. GRANT NUMBER

5c. PROGRAM ELEMENT NUMBER

6. AUTHOR(S)
Dr. James F. Ranville
Dr. Chris Muzny

5d. PROJECT NUMBER

5e. TASK NUMBER

5f. WORK UNIT NUMBER

7. PERFORMING ORGANIZATION NAME(S) AND ADDRESS(ES)
Department of Chemistry and Geochemistry
Colorado School of Mines
Golden, Colorado 80401

8. PERFORMING ORGANIZATION REPORT NUMBER

9. SPONSORING / MONITORING AGENCY NAME(S) AND ADDRESS(ES)
U.S. Department of the Interior, Bureau of Reclamation,
Technical Service Center, Environmental Services Division,
Water Treatment Engineering and Research Group, 86-68230,
PO Box 25007, Denver CO 80225-0007

10. SPONSOR/MONITOR'S ACRONYM(S)

11. SPONSOR/MONITOR'S REPORT NUMBER(S)
Report No. 102

12. DISTRIBUTION / AVAILABILITY STATEMENT
Available from the National Technical Information Service (NTIS),
Operations Division, 5285 Port Royal Road, Springfield VA 22161

13. SUPPLEMENTARY NOTES

14. ABSTRACT ***(Maximum 200 words)***

The reauthorization of the Safe Drinking Water Act in 1986 required the promulgation of several new treatment rules. The Surface Water Treatment Rule, the Enhanced Surface Water Treatment Rule), and the Total Coliform Rule were designed to eliminate the presence of harmful pathogenic organisms including: *Giardia lamblia, Legionella, Cryptosporidium,* fecal coliform, and *Escherichia coli*. The Disinfectants/ Disinfection By-Products Rule is intended to lead to removal of trihalomethanes and other disinfectant byproducts (DBPs) in drinking water by reducing the amounts of DBPs and/or removing DBP precursors such as natural organic matter found in source water supplies. Membrane technology is becoming an attractive alternative to conventional treatment to protect public health. Improving the economics process, through membrane design and an increase in use, drives the degree to which membrane treatment will become established in the United States. Increase in use has created new knowledge and experience with membrane treatment of drinking water and reclaimed wastewater, which induce further installations of membrane treatment systems. It is anticipated that during the next 10 to 40 years membranes will be integrated into almost all water treatment processes. This report discusses the various field flow filtration processes, fractionation, and solute membrane interaction, and a comparison of the various models studied.

15. SUBJECT TERMS
flow field flow fractionation, reverse osmosis, seawater, solute, analysis, membrane, model

16. SECURITY CLASSIFICATION OF:			**17. LIMITATION OF ABSTRACT**	**18. NUMBER OF PAGES**	**19a. NAME OF RESPONSIBLE PERSON**
UL					Michelle Chapman
a. REPORT	**b. ABSTRACT**	**c. THIS PAGE**		36	**19b. TELEPHONE NUMBER** *(include area code)*
					303-445-2264

Desalination and Water Purification Research and Development Program Report No. 102

Predicting Membrane Flux Decline Using Parameters Derived from Field-Flow Fractionation Measurements

Prepared for Reclamation Under Agreement No. 01-FC-81-0738

by

Dr. James F. Ranville, Colorado School of Mines
Dr. Chris Muzny, NIST

U.S. Department of the Interior
Bureau of Reclamation
Technical Service Center
Environmental Resources Division
Water Treatment Engineering and Research Group
Denver, Colorado

June 2006

MISSION STATEMENTS

The mission of the Department of the Interior is to protect and provide access to our Nation's natural and cultural heritage and honor our trust responsibilities to Indian tribes and our commitments to island communities.

The mission of the Bureau of Reclamation is to manage, develop, and protect water and related resources in an environmentally and economically sound manner in the interest of the American public.

Disclaimer

Information contained in this report regarding commercial products or firms was supplied by those firms. It may not be used for advertising or promotional purposes and is not to be construed as an endorsement of any product or firm by the Bureau of Reclamation.

The information contained in this report was developed for the Bureau of Reclamation; no warranty as to the accuracy, usefulness, or completeness is expressed or implied.

Table of Contents

List of Figures

List of Figures (continued)

Acronyms and Abbreviations

cm	centimeter
cm^2	square centimeters
DBPs	disinfectant byproducts
DLVO	Derjagin and Landau and Verwey and Overbeek
DVE	dehydrated vegetable extract
FEM	finite element approach
FFF	flow field fractionation
ESWTR	Enhanced Surface Water Treatment Rule
Fl FFF	flow field flow fractionation
MF	microfiltration
MFI	modified fouling index
mL/min	milliliters per minute
MWCO	molecular weight cut off
NF	nanofiltration
nm	nanometer
NOM	natural organize matter
RO	reverse osmosis
RTD	residence time distribution
SDI	silt density index
SWTR	Surface Water Treatment Rule
TCR	Total Coliform Rule
THMs	trihalomethanes
UF	ultrafiltration
UVA	ultraviolet absorbance
%	percent

1. Introduction

For more than a century, United States public health has relied on the use of filtration to remove harmful components in drinking water. During this time, the design and operation of filtration processes has been constantly under further refinement. A relatively recent development is the use of membrane technology as an important component of a multiple stage approach to drinking water treatment. The growing, worldwide demand for safe drinking water, in a time when water resources are limited, will further drive the development of these technologies. Technologies developed in the industrialized world undoubtedly will find a market in developing countries as these nations seek to improve their water supplies.

In the United States, the reauthorization of the Safe Drinking Water Act in 1986 required the promulgation of several new treatment rules. The Surface Water Treatment Rule (SWTR), the Enhanced Surface Water Treatment Rule (ESWTR), and the Total Coliform Rule (TCR) were designed to eliminate the presence of harmful pathogenic organisms including: *Giardia lamblia, Legionella, Cryptosporidium,* fecal coliform, and *Escherichia coli*. The Disinfectants/ Disinfection Byproducts Rule is intended to lead to removal of trihalomethanes (THMs) and other disinfectant byproducts (DBPs) in drinking water by reducing the amounts of DBPs and/or removing DBP precursors such as natural organic matter (NOM) found in source water supplies. Given these more stringent regulations, membrane technology is becoming an attractive alternative to conventional treatmentto protect the public health. The degree to which membrane treatment becomes established in the United States, and even more so in poorer developing nations, depends on improving the economics of the process. New membrane design and an increase in membrane use over the past decade have led to the reduction of production costs. Furthermore, this increase in use has created new knowledge and experience with membrane treatment of drinking water and reclaimed wastewater. These factors induce further installations of

membrane treatment systems. It has been postulated that, during the next 10 to 40 years, membranes will be integrated into almost all water treatment processes (Martinez, 1999).

1.1 Membrane Filtration

Membranes are capable of removing a variety of materials from drinking water including dissolved species, colloids, and suspended particles. These materials exist over a broad size range as illustrated in figure 1.

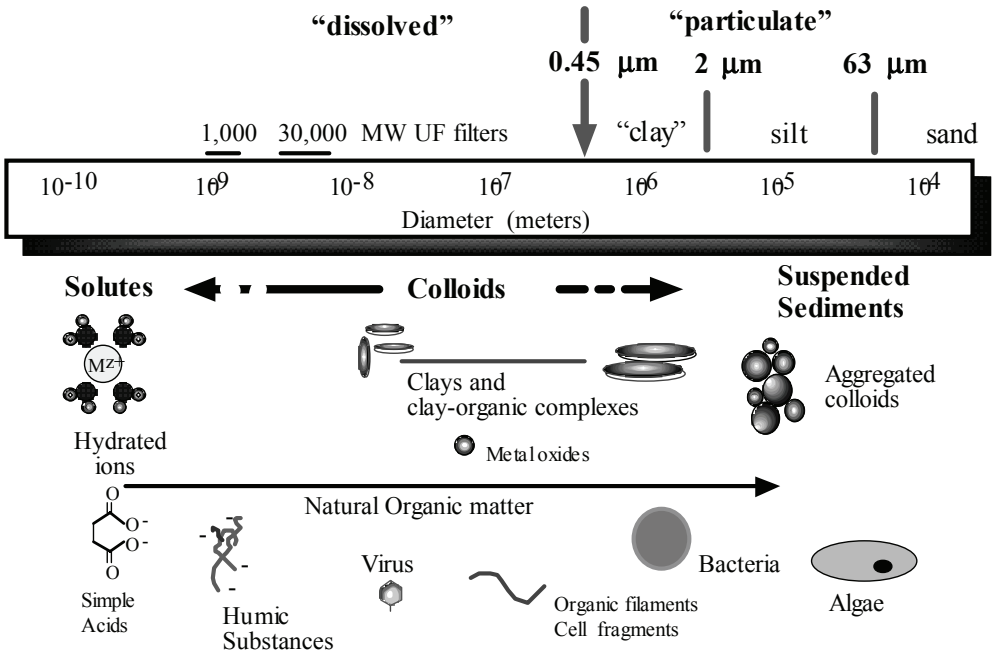

Figure 1. The size continuum of materials present as dissolved, colloidal, and particulate species in natural waters (Ranville and Schmiermund, 1997).

Filtration at 0.45 micron, which defines "dissolved" versus particulate while ignoring the presence of colloids, is commonly used. Further differentiation of particles into clay (less than 2 micrometers), silt (2-63 micrometers), and sand (greater than 63 micrometers) is commonly used to describe suspended sediments.

Undesirable dissolved compounds include: DBP precursors, toxic metals, trace organic contaminants, and nutrients. Colloidal contaminants include virus

particles, fine clays, colloidal iron and manganese, and colloidal organic matter. Problematic particulates include pathogenic bacteria, *Giardia lamblia, Cryptosporidium,* and suspended sediments that lead to turbidity.

Pressure-driven filtration is capable of removing submicron materials from the feed stream depending on the membrane pore size. Generally, pore sizes are described by the molecular weight cut off (MWCO) of the membranes. Membranes can be described as reverse osmosis (RO), nanofiltration (NF), ultrafiltration (UF) or as microfiltration (MF) depending on their MWCO. This is illustrated in figure 2 taken from Wright (2002) as adapted from Osmonics Inc. Reverse osmosis membranes were the first to be used in the drinking water industry for desalination of seawater in the 1960s (Anselme and Jacobs, 1996). Low-pressure membranes, including MF and UF, began to be applied by the water industry in the 1980s. NF membranes, while requiring lower operating pressures than RO membranes, provide a lower MWCO than MF or UF membranes. The work outlined in this report focused on NF membranes.

Low-pressure membranes provide the water industry with new means of meeting the requirements of drinking water regulations. They provide more options for reducing treatment costs when compared to conventional techniques. Low-pressure membranes used as post-treatment to conventional processes have been shown to reduce the disinfectant requirement and to serve as a promising component of a multiple-barrier treatment system design (Baker, 2000).

1.2 Membrane Fouling

The major challenge of membrane filtration lies in the fouling of membranes. Fouling reduces product water flux over time, requires expensive chemical cleaning, and if fouling is irreversible results in the need to replace the membrane (Howe and Clark, 2002). These problems increase the cost of membrane-based water treatment. The economics of using low-pressure membranes can be

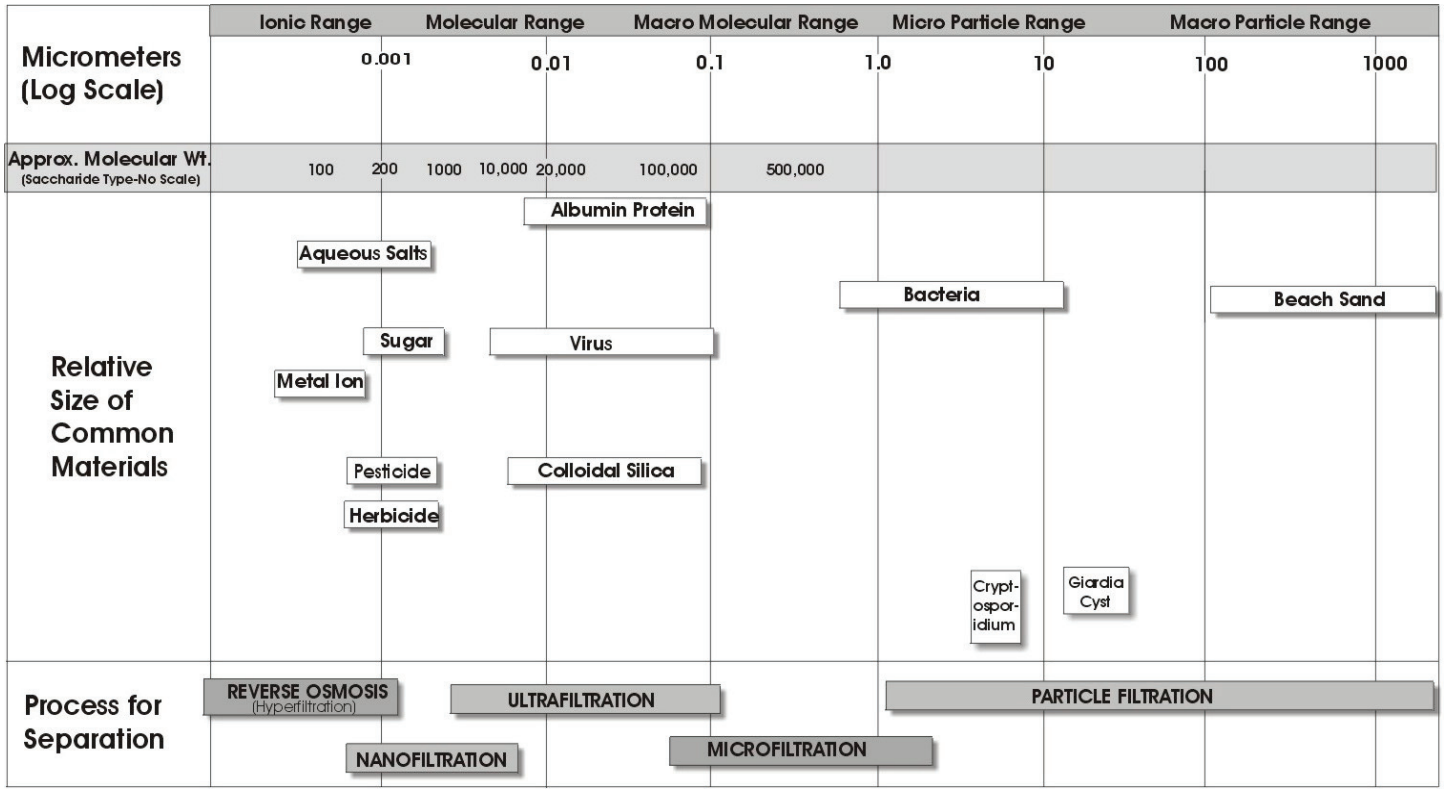

Figure 2. Types of pressure-driven filtration in relation to particle size, approximate MWCO, and commonly found materials.

Source: Wright (2002) as adapted from Osmonics Filtration Spectrum, Minnetonka, Minnesota.

significantly improved if better engineering solutions to reduce fouling and flux decline are developed. The major mechanisms of fouling are:

- Particulate fouling (cake formation) due to inorganic colloids and particles
- Organic fouling (adsorption) due to dissolved and colloidal organic matter
- Biofouling due to the attachment and growth of microorganisms
- Scaling in RO due to precipitation of salts (Brunelle, 1980)

The process of cake formation and adsorption depends on the nature of the source water and the properties of the membrane. Existing methods used to predict the flux decline potential of a given solution-membrane combination (e.g., turbidity, silt density index [SDI], and modified fouling index [MFI]) appear inadequate (Wright, 2002). It has been hypothesized that a set of simple tests can be used to characterize ("fingerprint") source (feed) waters and membranes such that integrating source water characteristics and membrane properties can lead to optimal membrane selection and operation (Pellegrino, personal communication). The rational for investigating the analytical separation technique of flow field flow fractionation (Fl FFF) as a "fingerprinting" tool will be described in detail.

1.3 Similarity of Tangential Flow Filtration and Flow Field Flow Fractionation

1.3.1 Tangential Flow Filtration

Most applications of membranes to water treatment use a tangential crossflow configuration as illustrated in figure 3. In this approach, the feed stream is passed over the surface of the membrane at a volumetric flow rate that is considerably higher than the permeate flow rate. The permeate flow is generated by the creation of a transmembrane pressure sufficient to overcome the membrane resistance. The crossflow creates shear which reduces both cake formation and the concentration of solutes near the membrane. Membranes are manufactured in two geometries: flat plate and cylindrical. The cylindrical geometry is illustrated in figure 3. Numerous more-detailed descriptions of crossflow filtration can be found elsewhere (Aptel and Buckley, 1996).

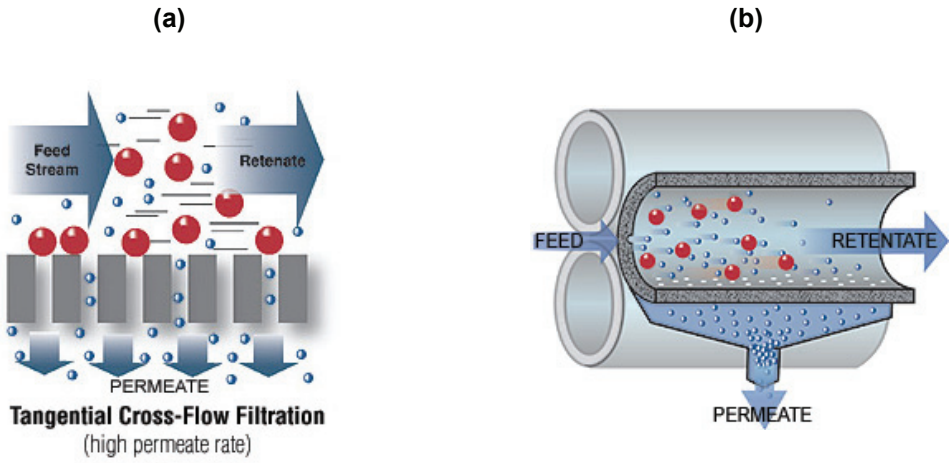

Figure 3. (a) The flow configuration used in tangential crossflow filtration and (b) an example of the cylindrical geometry of a commonly used membrane module (adapted from Spectrum Inc.).

The basic elements of crossflow filtration are similar in many respects to those of flow field flow fractionation. These similarities lead to the central hypothesis of this work: that measurements of processes occurring in Fl FFF analysis could be related to those occurring during crossflow filtration.

1.3.2 Flow Field Flow Fractionation

Field flow fractionation (FFF) represents a family of techniques that were developed as an analytical tool to separate and determine the size of solutes using flow in very thin channels (Giddings, 1966, 1987, and 1993). Martin and Williams (1992) provide a summary of how FFF leads to separation of solutes contained in a solvent and how this information is used to obtain size information. Typical 'fields' include thermal, electrical, gravitational, and fluid crossflow. Flow FFF (Fl FFF) is the most universally applicable FFF technique, and its basic features are shown in figure 4. In the case of Fl FFF, the channel is constructed of porous walls to allow a crossflow of solvent. It can be considered that Fl FFF is an idealization of crossflow filtration. It has a constant channel and cross-field flow that provides hydrodynamic conditions that are qualitatively similar to crossflow filtration but are more constant, consistent, and predictable.

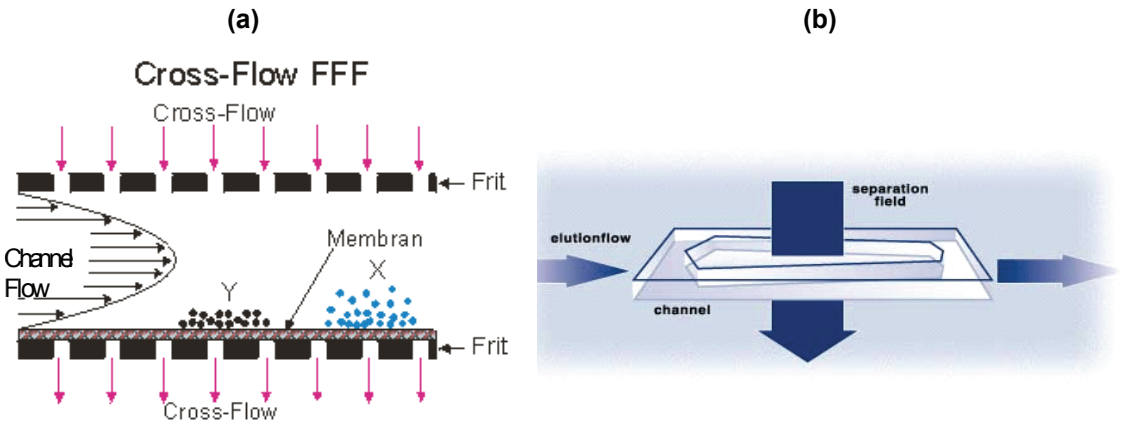

Figure 4. (a) Schematic cross-sectional representation of the processes occurring within a Fl FFF channel which cause separation. (b) Typical configuration of Fl FFF showing the similarity to flat plate crossflow filtration membrane systems.

Source: Adapted from PostNova Analytics Inc.

Additionally, the presence of a membrane, required to prevent loss of solutes through the lower porous wall of the Fl FFF channel bears similarity to a crossflow filtration module.

The classical use of FFF has been to perform separations based on the degree of interaction of a solute with the applied field. In Fl-FFF, the applied field forces sample components to the lower wall. Back diffusion of sample components arises from the increase in concentration at the lower wall and creates a force that opposes the applied field. At equilibrium, the field induced by the velocity of the crossflow is balanced by the back diffusion. Laminar flow down the channel moves solutes through the system in a manner analogous to the retentate flow in crossflow filtration. The velocity of this flow varies across the width of the channel and is described by a parabolic distribution. This results in separation of solutes based solely on differences in the diffusion coefficient for each component of the sample mixture. For the example shown in figure 4, component X has a higher diffusion coefficient than component Y and, thus, has a higher equilibrium position above the wall. This results in X interacting with higher velocity flow lines than Y. The result is that the residence time in the Fl FFF channel is shorter than that for Y. The basic measurement in FFF is the average residence time (t_r)

of the solute as compared to the time required for displacement of the void volume (t_0). From this information, the first moment (mean) of the solute diffusion coefficient distribution can be calculated.

1.4 Flow Field Flow Fractionation Basic Theory

The equilibrium concentration distribution of a solute in the FFF channel decreases exponentially from the membrane when a solute is introduced to the Fl FFF channel. The constant ℓ, which represents the average distance above the wall, which arises from a balance of the field (crossflow velocity) versus the rate of back diffusion of the solute, is given as:

$$\ell = \frac{D_c}{\left|U_{field}\right|} \tag{1}$$

where D_c is the diffusion coefficient of the solute [cm^2-s^{-1}] and U_{field} is the velocity of the cross field applied to the solute [cm-s^{-1}]. Giddings also defined a retention parameter, λ, as a convenient and dimensionless parameter for the 'ℓ' constant in a Fl FFF field as:

$$\lambda = \frac{\ell}{w} \tag{2}$$

where w is channel thickness [centimeter (cm)]. Thus, it can be shown that:

$$\lambda = \frac{\ell}{w} = \frac{D_c}{\left|U_{field}\right| w} = \frac{D_c V^o}{V_c w^2} \tag{3}$$

where V_c is the cross field volumetric flow rate and V^0 is the channel volume.

The Stokes-Einstein equation relating particle diameter with its diffusion coefficient can apply to the Fl-FFF system (Williams et al., 1997) and thus:

$$D_c = \frac{kT}{3\pi\eta d_{St}} \tag{4}$$

where, D_c is the Stokes-Einstein diffusion coefficient, k is the Boltzmann constant, T is the absolute temperature, d_{St} is the Stokes-Einstein diameter of a spherical particle, and η is the eluant viscosity.

As a result, it follows that retention in Fl FFF is related to diameter by:

$$\lambda = \frac{\ell}{w} = \frac{kTV^0}{3\pi\eta V_c w^2 d_{St}} \tag{5}$$

Under ideal conditions, the relative velocity (or retention ratio), R, of a solute in the channel is the ratio of the solute velocity, u_{sample}, to the eluant velocity $\langle v \rangle$:

$$R = \frac{u_{sample}}{\langle v \rangle} \tag{6}$$

The velocities are related to the channel length (L) and the average residence time of the eluant, t_0, and the solute, t_r, by $u_{sample} = \frac{L}{t_r}$ and $\langle v \rangle = \frac{L}{t_0}$, respectively.

Giddings (1968) related the relative velocities to the FFF parameter, λ, for a parallel plate channel under the influence of an eluant with a parabolic flow profile.

$$R = \frac{t_0}{t_r} = 6\lambda\left[\coth\left(\frac{1}{2\lambda}\right) - 2\lambda\right] \tag{7}$$

Thus, the diffusion coefficient and particle diameter of a solute can be determined experimentally through the relationship of the retention ratio (R) and λ.

1.5 Non-Ideal Behavior in Fl FFF as a Measure of Solute-Membrane Interaction

The fundamental principle underlying classical applications of Fl FFF to size analysis and size-based separations is that λ depends solely on the balance of diffusion and the applied field. However, other potential interactions of either an attractive or repulsive nature can occur between the solute and the membrane as illustrated in figure 5. Repulsive electrostatic interactions create an additional force (F_{EL}) that causes the solutes to occupy a position further above the membrane surface than predicted by the solute diffusion coefficient. Attractive interactions such as van der Waals forces (F_{VDW}) and less commonly, attractive electrostatic interactions, cause the opposite effect. Use of a surfactant and selection of an appropriate carrier ionic strength and pH minimizes these interactions. These perturbations in the behavior of solutes in an Fl FFF channel are considered nuisances in the FFF community, as the goal is usually to obtain an accurate measurement of the solute diffusion coefficient or diameter (1st moment of the residence time distribution (RTD). Giddings (1997) and Martin (1999) completed a mathematical analysis of the error due to these perturbations. The Derjagin, Landau, Verwey, and Overbeek (DLVO) theory was used to consider the effects of electrostatic forces and van der Waals forces between solutes and

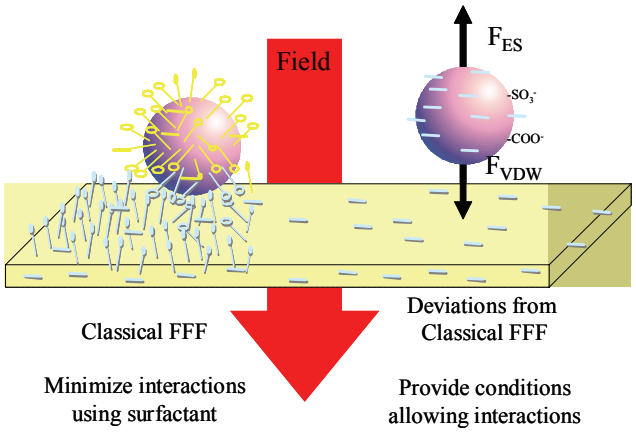

Figure 5. Schematic showing "ideal" behavior of a solute when surfactant is present as compared to situations where interactions due to electrostatic (F_{EL}) and van der Waals (F_{VDW}) forces perturb the equilibrium height (ℓ) (Wright, 2002).

the channel wall regardless of the field (electric, gravitational, thermal, or flow). Williams et al. (1997) identified and developed semi-empirical relationships between solute retention ratio and sources of error.

What is considered a problem in classical Fl FFF analysis is an opportunity to investigate solute-membrane interactions. The flux decline potential of a solution during crossflow filtration is related to the potential for solutes forming a boundary layer or cake-like mass and their potential for irreversibly adhering to the membrane. The qualitative relationships that define a solution's potential for causing flux decline relate to the physical properties of the solute (diameter, molecular weight) and the interactions between the solute and the membrane. These same properties govern the Fl FFF analysis under non-ideal conditions. Thus, Fl FFF may be a useful tool for defining the observed properties of a solution that is being filtered, with the results being interpreted in terms of the parameters in a flux decline model. Of course, there are other factors that can affect flux, including module configuration, flow hydrodynamics, and operating procedures (such as hydraulic backwashing). However, further understanding of solute-membrane interactions will improve our ability to make appropriate selections of membrane-source water combinations.

The previous discussion described how solute diameter (molecular weight) and solute-membrane interactions affect the Fl FFF measurement of the 1^{st} moment (mean) of the residence time distribution of the solute within the Fl FFF channel. Additional useful data might be obtained by examining the entire RTD of solutes eluted from the Fl FFF channel. It has been suggested that a more detailed moment's analysis of Fl-FFF RTDs can potentially yield relationships important to describing solute properties that can affect membrane fouling (Wright, 2002). These descriptors of the RTDs include the variance (2^{nd} moment), skew (3^{rd} moment), and kurtosis (4^{th} moment).

The basic approach taken is to compare an "ideal" RTD to that obtained under conditions that allow solute-membrane interactions. From the comparison of the

moments of these two distributions, information will be extracted that can be used to parameterize a flux-decline model that accounts for solute-membrane interactions. It is very difficult to obtain the "ideal" RTD for a solute even when solution conditions are manipulated to minimize interactions. An alternative approach is to obtain the "ideal" RTD through numerical modeling of the expected behavior of a solute in the Fl FFF channel. The approach for predicting the entire RTD is somewhat more involved than that previously described for obtaining the mean of the RTD. However, it is critical that an accurate prediction for the "ideal" RTD be obtained to interpret the "perturbed" RTD.

2. Materials and Methods

2.1 Fl FFF Instrumentation

The FFF method under consideration here is known as symmetric Fl FFF. The basic configuration is depicted in figure 6, and the specific experimental apparatus is shown in figure 7. The instrument used was an F-1000 Universal Fractionator (PostNova Analytics LLC, Salt Lake City). A long channel with dimensions of approximately 2.5 cm wide, 25 cm long and 0.025 cm thick is used. Two pumps supply the channel and crossflows. The flow down the channel will be based on using a "standard" membrane in all evaluations of source water-membrane combinations (J. Pelligrino, personal communication).

The particular system used in this study is novel in that multiple detectors were used to measure the concentrations of the solutes as they eluted from the Fl FFF channel. For this study, only the ultraviolet absorbance (UVA) and fluorescence (fl) detectors were used to produce the desired RTDs. The addition of a total organic carbon detector, while not used in this project, shows great promise in characterizing organic matter foulants (Ullmann et al., 2000).

2.2 Solutes and Operating Conditions

It has been suggested that a standard solute mixture consisting of three components be used to examine solute-membrane interactions (Wright, 2002). These components would represent the types of materials likely to be found in natural waters. Uniform colloidal silica could represent inorganic mineral colloids. In this study, Snowtex ZL (Nissan Chemicals, Tokyo, Japan) having a mean diameter of 118 nanometers (nm) was used. The original suspension was dialysed against deionized water using an 8000 MWCO membrane (Wright, 2002). To represent macromolecular materials, a whey protein (PowerPro, Land O'Lakes, Arden Hills, Minnesota, United States) was selected. This material was obtained as a powder, and suspensions were prepared just prior to

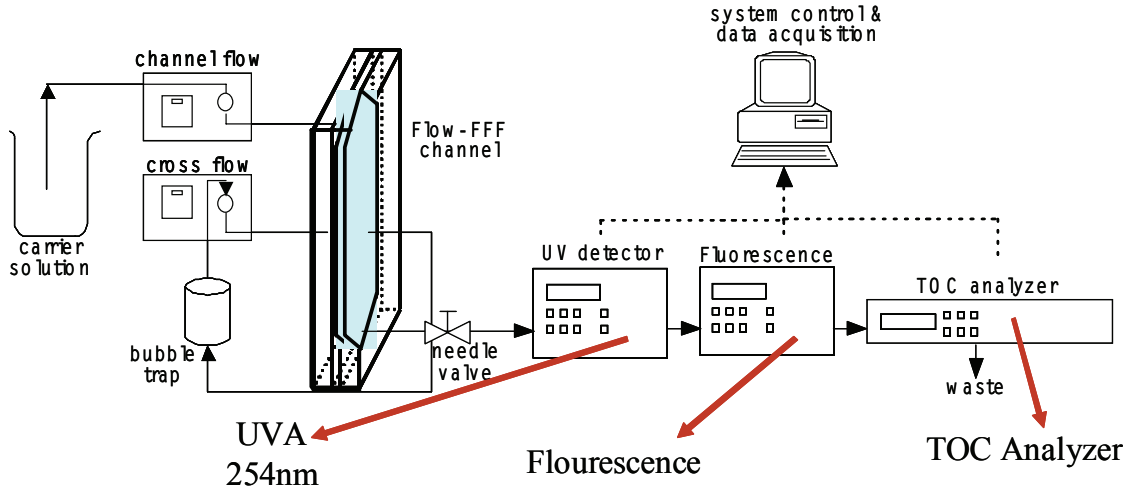

Figure 6. Configuration of the FI FFF system including the use of multiple detectors.

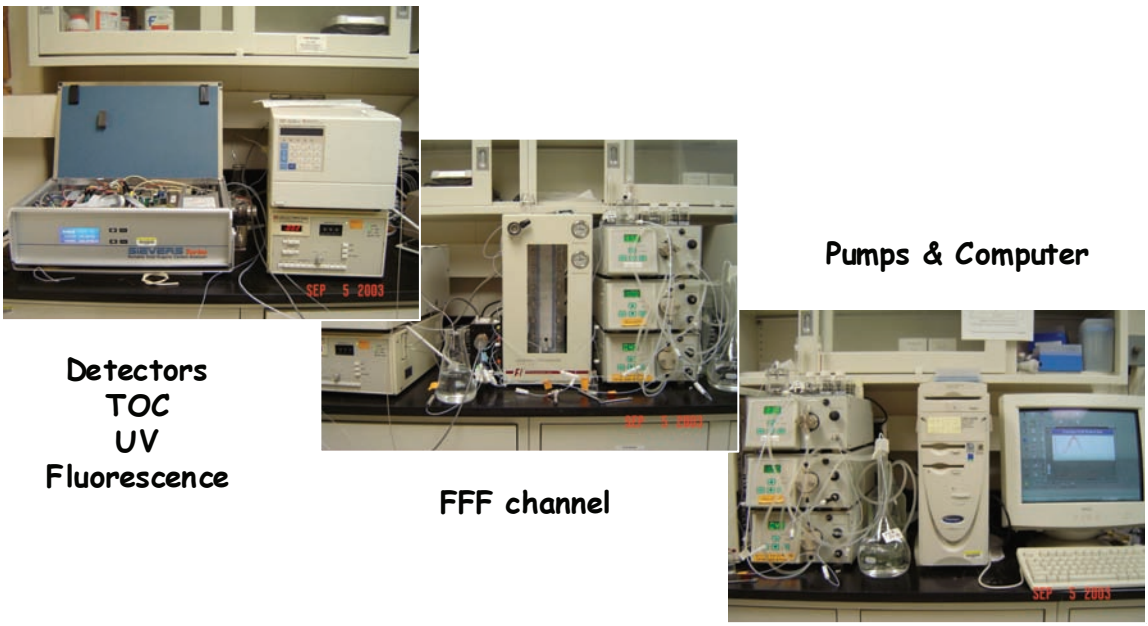

Figure 7. FI FFF apparatus showing the arrangement of computer, pump, F-1000 module, and multiple detectors.

experimentation. A third component, present to represent low molecular weight dissolved organic matter, was a dehydrated vegetable extract (DVE) (Frontier™, Norway, Iowa, United States). Experiments with this material are not described in this report. Additional experiments were performed with monodisperse polystyrene beads (Duke Scientific), but the results are not reported.

The channel flow rates used in the experiments ranged from 1-2 milliliters per minute (mL/min). For data reported here, a channel flow rate of 1.5± 0.1 mL/min was used. Crossflow rates varied depending on the material under investigation. For colloidal silica, the crossflow rates ranged from 0 to 1.5 mL/min. For the whey protein, the crossflow rates ranged from 0 to 5 mL/min. Carrier compositions ranged in ionic strength from 0 to 0.001 molar solution of potassium chloride. Experiments were performed with and without surfactant. For the results presented in this report, the carrier solutions contained the surfactant FL-70 (Fisher Scientific) at a concentration of 0.001 percent (%).

Flourescence detection was used for both the silica and the whey protein. For silica, the exitation/emission wavelengths were 350/365 nm. For the whey, a combination of 280/330 nm was used.

2.3 Development of RTD Models

The purpose of this section is to outline the application of two separate modeling techniques for describing the Fl FFF separation process. The fundamental equations describing flow of analytes in the channel will first be described, and then two distinct methods—finite element modeling and analytical approximation using center-manifold theory—will be described. The usefulness and applicability of each method will be described. Both methods will then be compared with experimental data to determine if either truly is applicable to this system.

The fundamental equations for modeling separation in an FFF channel can be broken into two parts. First, the equations for modeling the solvent flow in the channel are the Navier-Stokes equation together with the continuity equation, which for incompressible flow are:

$$\frac{\partial \mathbf{q}}{\partial t} + (\mathbf{q} \cdot \nabla)\mathbf{q} = -\frac{1}{\rho}\nabla p + \frac{\eta}{\rho}\nabla^2 \mathbf{q} \tag{8}$$

$$\nabla \cdot \mathbf{q} = 0 \tag{9}$$

where p is the pressure, ρ is the density, η is the viscosity and $\mathbf{q} = u_x(x,y,t)\mathbf{i} + u_y(x,y,t)\mathbf{j}$ is the velocity field for the solvent. Second, the equation for modeling the flow of the analyte is the advection-diffusion equation:

$$\frac{\partial c}{\partial t} + \mathbf{q} \cdot \nabla c = \kappa \nabla^2 c \tag{10}$$

where $c(x,y,t)$ is the concentration of the analyte as a function of position down the channel x, position across the channel y and time t, and κ is the analyte diffusivity (figure 8).

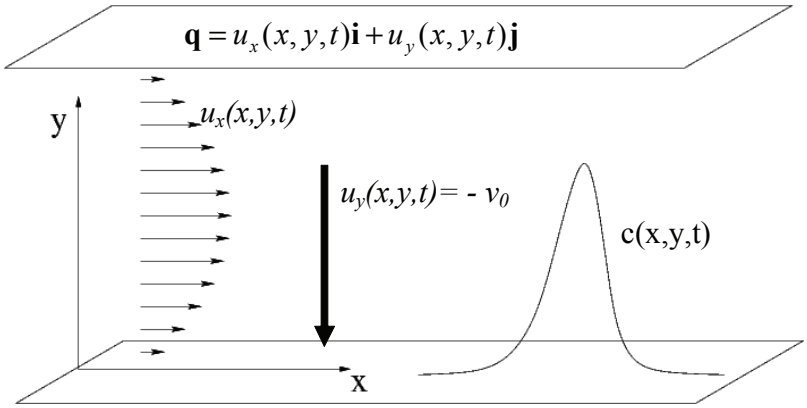

Figure 8. The geometry for the symmetric FFF channel is shown with the actual dimensions exaggerated for clarity. The true channel height is ~1,000 times smaller than its length. The vector field that describes the flow of the solvent is q(x,y,t). The field describing the analyte concentration at all positions in the channel is c(x,y,t).

The boundary conditions for solvent flow if the crossflow velocity is v_0 and the channel width is b are $u_x = 0$ and $u_y = -v_0$, at $y = 0$ and b. The boundary conditions for $c(x,y,t)$ are zero flux at the upper and lower plate which can be expressed as:

$$v_0 c + \kappa \frac{\partial c}{\partial y} = 0, \text{ at } y = 0 \text{ and } b. \tag{11}$$

At this point, it is reasonable to rescale the lengths and times used in these equations to ones appropriate for this problem. The scaled variables are $\tilde{x} = x / x_{sc}, \tilde{y} = y / y_{sc}, \tilde{t} = t / t_{sc}$, where the *sc* subscript indicates a scaling parameter. The following scaling parameters are used:

$$y_{sc} = \kappa / v_0 \ , \ x_{sc} = \kappa / v_0$$

For steady solvent flow, the Navier-Stokes equation can be solved analytically for these boundary conditions to determine the solvent velocity field. The solutions are:

$$\begin{aligned} u_y(x,y,t) &= -v_0 \\ u_x(x,y,t) &= \frac{2u_0\sigma}{\bar{v}} \ \frac{1-\exp(-y/\bar{y}\sigma)}{1-\exp(-\bar{v}/\sigma)} - \frac{y}{\bar{y}} \end{aligned} \qquad (12)$$

where $\bar{y} = \kappa / v_0$ is the characteristic length for the analyte distribution across the channel, $\bar{v} = v_0 b / \kappa$ is the cross channel Peclet number, $\sigma = \frac{\eta}{\kappa\rho}$ is the Schmidt number, $u_0 = -\frac{\partial p}{\partial x} \ \frac{\bar{y}b}{2\eta} = \frac{6\bar{u}}{\bar{v}}$ is the velocity of solvent in the boundary layer expressed in terms of the average channel flow rate $\bar{u} = -\frac{\partial p}{\partial x} \ \frac{b^2}{12\eta}$. This solution assumes a constant down channel pressure drop with zero tangential flow at the surfaces. In the limit of small $\bar{v}/\sigma = \frac{v_0\rho b}{\eta} \equiv R_c << 1$, where R_c is the crossflow Reynolds number, this becomes:

$$u(y) \approx u_0 \ \frac{y}{\bar{y}} - \frac{y}{\bar{y}}^2 \frac{1}{\bar{v}} + \frac{y}{\bar{y}\sigma} \ \frac{\bar{v}}{6} - \frac{y}{2\bar{y}} + \frac{y}{\bar{y}}^2 \frac{1}{3\bar{v}} + \vartheta \frac{\bar{v}^2}{\sigma^2} \qquad (13)$$

which is the expected parabolic velocity profile correct to second order in $\frac{\bar{v}^2}{\sigma^2}$.

The value $v_0 = \frac{f_{cc}}{60 A_{cc}}$, where f_{cc} is the cross-channel flow rate in mL/min and A_{cc} is the surface area of the channel or about 25 cm x 2.5 cm = 62.5 cm^2. So using the known experimental values $\frac{\bar{v}}{\sigma} \approx \frac{f_{cc} b \rho}{60 A_{cc} \eta} \approx \frac{f_{cc} 2 \cdot 10^{-5}}{3}$, which will be small for all crossflow rates of interest.

At this point, a mathematical model has been completely defined for the evolution of the analyte concentration $c(x, y, t)$ in the channel during a separation experiment. The problem is specified by equation 10 together with boundary conditions equation 11 and the solution for the solvent flow field $\mathbf{q} = u_x(x, y, t)\mathbf{i} + u_y(x, y, t)\mathbf{j}$ as presented in its exact form in equation 12 or an approximate form in equation 13. There is no known analytical solution for equation 10, so methods of approximation must be employed. The two methods considered here are numerical solution via finite element techniques and an approximate analytical solution using center-manifold theory as originally presented by Suslov and Roberts (1999).

To get an approximate solution to the problem of analyte flow down the channel, Suslov and Roberts used the center-manifold theory which starts with the observation that, in the absence of a down channel flow, the distribution quickly relaxes to:

$$c(x, y, t) = C(x, t) \exp(-y / \bar{y}) \tag{14}$$

where $C(x, t)$ is the concentration along the bottom of the channel. An approximate solution is then determined completely by solving a time-dependent partial differential equation for $C(x, t)$ and then using the expression:

$$c(x,y,t)=\frac{\exp(-y/\bar{y})}{\bar{y}}\left\{C(x,t)+\frac{\partial C}{\partial t}\frac{\tau y}{\bar{y}^2}\left[\left(1-\frac{1}{\sigma}\right)\left(\frac{3+y/\bar{y}}{3\bar{v}}-\frac{1}{2}\right)-\frac{(\bar{v}-y/\bar{y})^2}{12\bar{v}\sigma}\right]\right\} + \vartheta\left(\frac{\partial^2 C}{\partial x^2},\frac{\bar{v}^2}{\sigma^2},e^{-\bar{v}}\right) \quad (15)$$

to find the complete concentration profile. Suslov and Roberts (1999) showed that, when $\frac{\partial^2 C}{\partial x^2},\frac{\bar{v}^2}{\sigma^2}$ and $e^{-\bar{v}}$ are much less than one, the surface concentration is determined by solution of the one-dimensional advection-diffusion equation

$$\frac{\partial C}{\partial t}=-U\frac{\partial C}{\partial x}+D\frac{\partial^2 C}{\partial x^2}, \quad (16)$$

with the effective advection speed U and diffusion coefficient D given by

$$U=\frac{6\bar{u}\kappa}{v_0 b}\left(1-\frac{2}{\bar{v}}+\frac{1}{\sigma}\left(\frac{\bar{v}}{6}-1+\frac{2}{\bar{v}}\right)+\vartheta\left(\frac{\bar{v}^2}{\sigma^2},e^{-\bar{v}}\right)\right) \quad (17)$$

$$D=\frac{72u^{-2}\kappa^3}{v_o^4 b^2}\left(\left(\kappa^2+2-\frac{20}{\bar{v}}+\frac{56}{\bar{v}^2}\right)+\frac{2(\bar{v}-8)}{3\sigma}\left(1-\frac{12}{\bar{v}}+\frac{42}{\bar{v}^2}\right)+\vartheta\left(\frac{\bar{v}^2}{\sigma^2},e^{-\bar{v}}\right)\right) \quad (18)$$

The solution of equation 16 will lead to a complete description of the analyte concentration in the channel. For the special case where the initial condition is that of a Gaussian profile with width *s* on the bottom of the channel, equation 16 can be solved explicitly.

$$C(x,t=0)=C_0\exp(-x^2/2s^2) \quad (19)$$

$$C(x,t)=\frac{1}{\sqrt{\pi}\sqrt{4Dt+s^2}}\exp\left(-\frac{(x-Ut)^2}{4D+s^2}\right). \quad (20)$$

Finally, a combination of equation 20 with equation 15 gives a complete solution for $c(x,y,t)$. Using this, we can then simulate experimental conditions. There are two important issues to note. The first is about normalization. The

concentration $c(x,y,z,t)$ is normalized so that its integral over the entire channel is one. For the case of an initial Gaussian profile in x, exponential decay in y and constant in z, since

$$\frac{1}{ws\bar{y}\sqrt{\pi}}\int_{-\infty}^{\infty}\int_{0}^{b}\int_{0}^{w}\exp(-y/\bar{y})\exp\left(-\left(\frac{x^2}{s^2}\right)\right)dz\,dy\,dx = 1,$$

$$c(x,y,z,t=0) = \frac{1}{ws\bar{y}\sqrt{\pi}}\exp(-y/\bar{y})\exp\left(-\left(\frac{x^2}{s^2}\right)\right). \qquad (21)$$

Second, while the concentration profile as a function of time gives all the relevant information for the problem, it is not what is measured in an experiment. Experimentally, the analyte *flux* off the channel (in the x direction), not its instantaneous concentration, is the measured quantity.

$$F_{tot}(x,t) = \int_{\substack{Channel\\ Cross-section}} J_x(x,y,z,t)\,dA = \iint\left(c\,u_x - \kappa\frac{\partial c}{\partial x}\right)dy\,dz \qquad (22)$$

The quantity of interest is the concentration in the flow stream out of the channel as a function of time, $c_{stream}(t) = F_{tot}(x=l,t)/F_{down}$, where F_{down} is the solvent down-channel volumetric flow rate in cubic centimeters per second (cm^3/s) and l is the channel length. The final result is $c_{stream}(t)$, and it can be calculated *analytically* for the special case of an initial Gaussian profile.

The analytical result, while complicated to write down, has many advantages over numerical solutions. It is very easy, for instance, to integrate over a particle size distribution. It is also possible to optimize the flow rate for resolution of particles of a given size. However, it is not possible to consider variations in initial particle distribution in the channel or to include the possibility of other interactions. For this, we turn to finite element methods.

3. Results and Discussion

3.1 Comparison of Models

The model outputs for the two approaches are compared in figure 9. The equation being solved using the finite element approach (FEM) is equation 10 together with the boundary conditions (equation 11) and the velocity field (equation 12). These are discretized on a self-adjusting grid using the software package FLEXPDE. A particle diameter of 120 nm, chosen to approximate the silica, was input. Two crossflows were input (0.4 and 1.0 mL/min). The analytical approach (Suslov and Roberts, 1999) is also shown on figure 9. Both models yield comparable results.

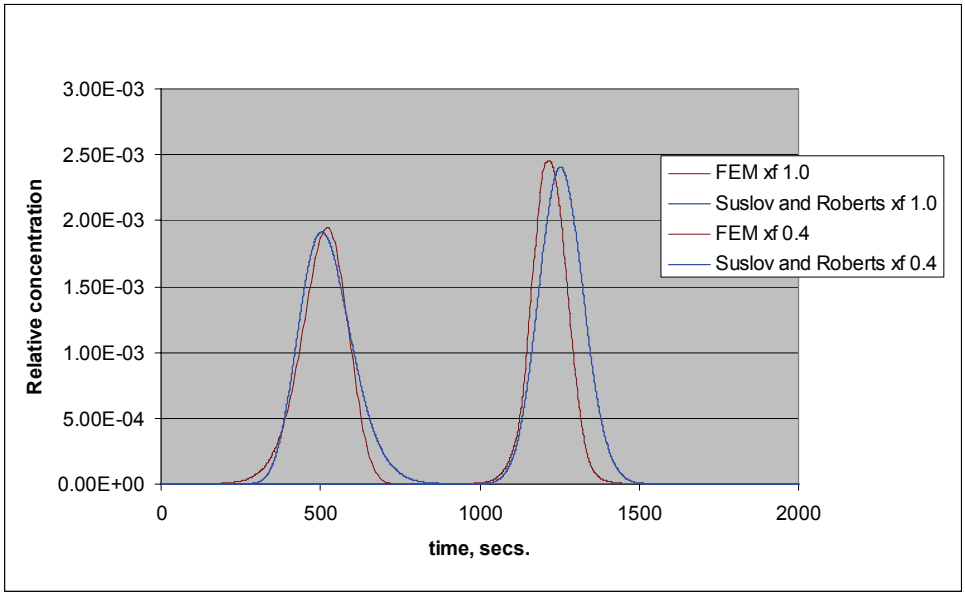

Figure 9. Comparison of model computed RTDs using a finite element and analytical solution. Input particle diameter = 120 nm and crossflows of 0.4 and 1.0 mL/min.

3.2 Comparison of Model and Experimental Results

The results of the analytical (Suslov and Roberts, 1999) and the experimentally determined RTDs for the silica particles are shown in figure 10 a and b. The model results were obtained using a particle diameter of 120 nm.

(a)

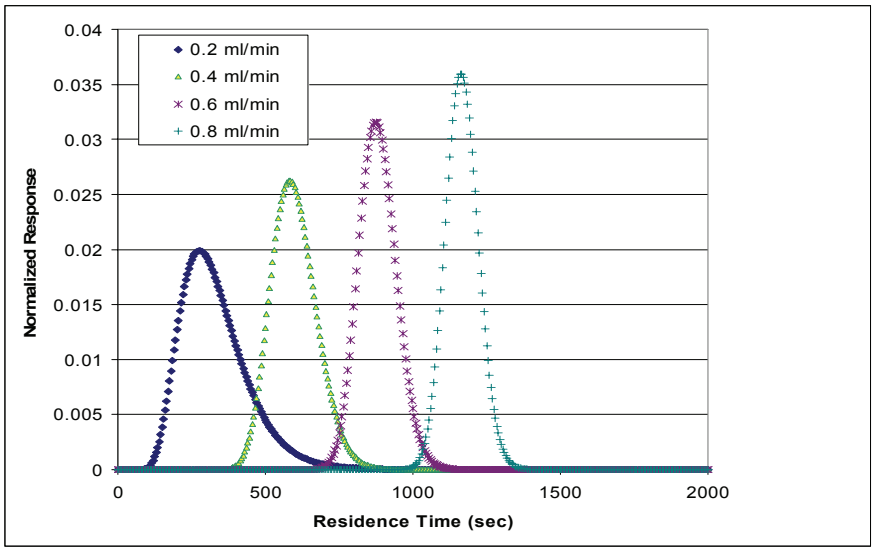

(b)

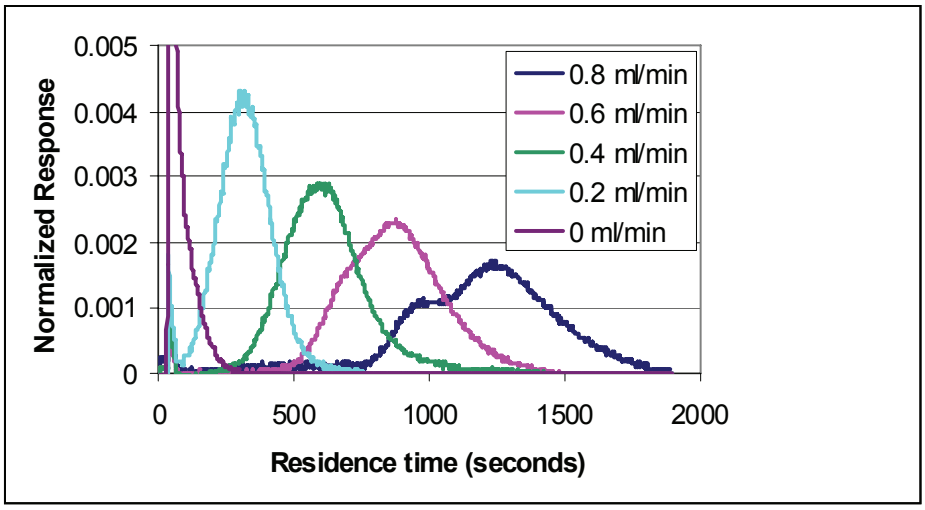

Figure 10. (a) RTD computed using the analytical (Suslov and Roberts, 1999) approach; (b) experimentally determined RTD for colloidal silica.

Both the model and the experimental data show the expected increase in the 0^{th} moment of the distribution (mode or peak max). However, the striking difference between the model and the experiment is in the peak width. These results are further illustrated in figure 11. The peak width in seconds, measured at one-half the peak max, is seen to increase for the experiment while decreasing for the model. The reason for the narrowing of the model can be understood

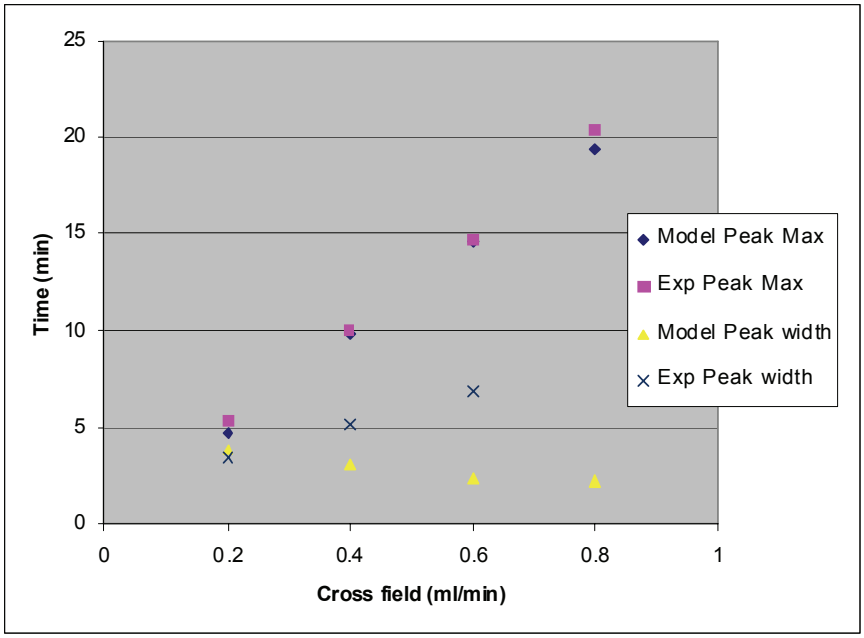

Figure 11. Comparison of the peak max and the width of the peak for silica obtained from the analytical model and experimentally.

conceptually by considering the position of the particles in the channel under variable fields. As the field is increased (i.e., higher crossflow rates), the particles occupy positions closer to the membrane surface, and the range of crossflows over which the exponential distribution of particles extends is smaller. Thus, the model predicts a narrowing of the RTD. In contrast, the observed experimental distribution becomes broader. The questions are: does this difference represent the looked for effect of solute-membrane interactions; and if so, can parameters be extracted from a comparison of the moments of the RTDs? As the particles are forced closer to the membrane under the higher crossflows, the potential for solute-membrane interactions indeed are likely to increase. However, these experiments were performed using a carrier containing 0.01 % FL-70 surfactant. Although it is likely impossible to experimentally produce an "ideal" RTD, the conditions used should have greatly limited solute-membrane interactions.

The observed differences may be explained by the increase in resolution of Fl FFF as the field is increased. As the field is increased, small differences in particle diameter lead to greater differences in retention time. If the silica is not truly monodisperse, then an increasing breadth of the RTD could be explained by

the improved resolution at higher fields as illustrated in figure 12. An absolute measurement of the silica polydispersivity was not made. To determine if a qualitative agreement between the model and experiment could be made by including polydispersivity, the model was run for a log-normal distribution of particle sizes with an assumed polydispersivity of 15%. As can be seen in figure 12, the experimentally observed broading of the RTDs as the field is increased is now seen in the model results as well. It appears that including polydispersivity into the model is required to produce model results that match experiments performed under "ideal" conditions.

A similar comparison between model and experimental results was made for whey protein and the results given in figure 13. In this case, the agreement between the model, without any estimated polydispersivity, and experimental results was better. This might be due to a narrower inherent distribution of molecular weights of the whey. Alternatively, the results may suggest that the resolution of the experimental measurements was insufficient to separate the individual components of the whey, which are much smaller than the silica particles.

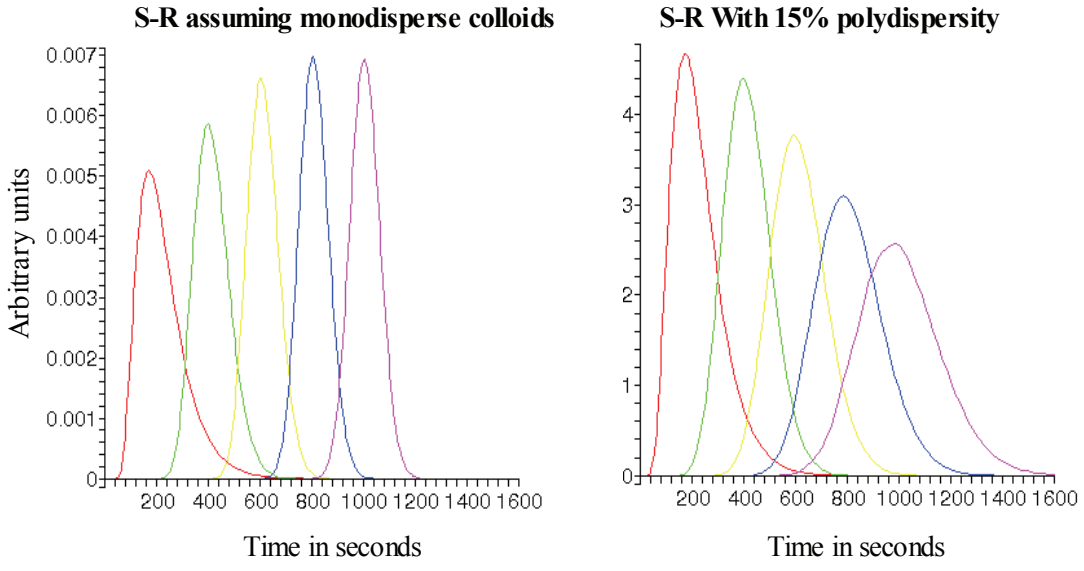

Figure 12. Influence of polydispersivity on the width of the model-computed RTDs. Model inputs were: crossflow rate = 1.4 mL/min, mean particle diameter = 100 nm, relative standard deviation of 0.15 (assuming a log-normal distribution).

(a)

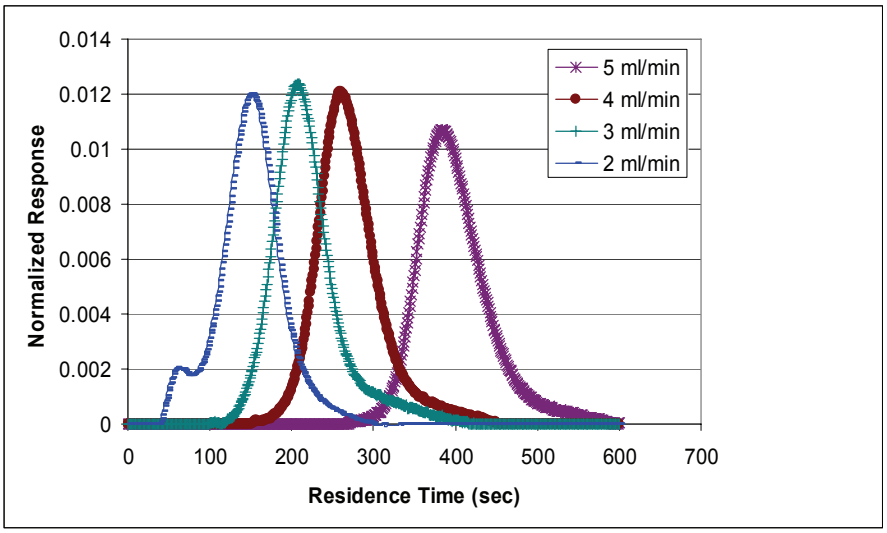

(b)

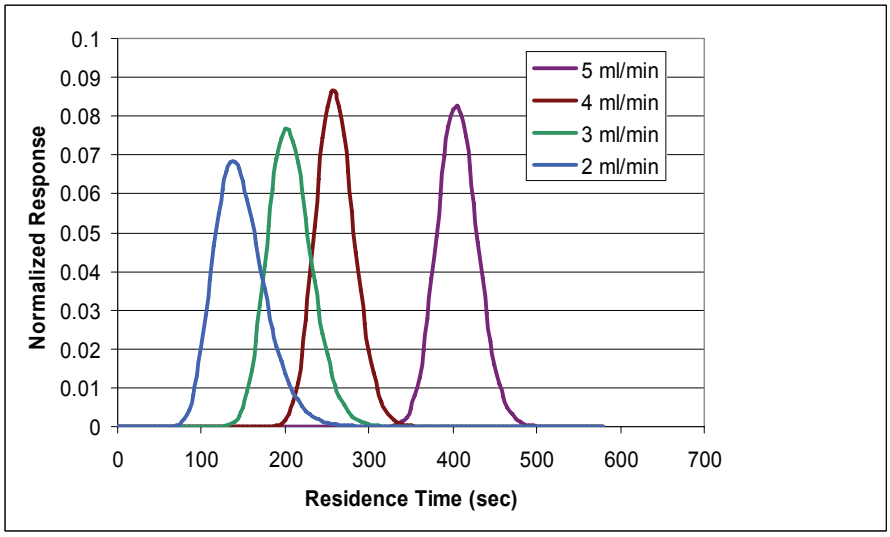

Figure 13. (a) Model computed RTDs for whey protein and (b) experimentally measured RTDs under crossflows of 2 to 5 mL/min.

3.3 Suggested Future Research

The analytical model first developed by Suslov and Roberts (1999) appears to provide a accurate "ideal" RTD distribution of solutes in the Fl FFF channel if polydispersivity is included in the calculations. This is suggested by the favorable comparison to esperimental results obtained using surfactants in the carrier

solution. The next step should be to continue obtaining experimental RTDs under variable solution compositions. From the measurements, parameters describing the deviation of the real and ideal RTD which describe solute-membrane interactions could be extracted. Simultaneously, measurements of flux decline need to be performed under similar solution compositions. From these two data sets, the ability of Fl FFF measurements to provide input into a flux decline model that accounts for solute-membrane interactions can be evaluated.

4. References

Anselme, C. and E. Jacobs, 1996. "Ultrafiltration, Chapter 10" in, *Water Treatment Membrane Processes*, J Mallevialle, P. Odendaal, and M. Weiser (eds), McGraw-Hill, New York.

Aptel, P. and C. Buckly, 1996. "Catagories of membrane operations, Chapter 2" in, *Water Treatment Membrane Processes*, J Mallevialle, P. Odendaal, and M. Weiser (eds), McGraw-Hill, New York.

Baker, R.W., 2000. *Membrane Technology and Applications*, McGraw-Hill Publishers.

Brunelle, M.T., 1980. "Colloidal Fouling of Reverse Osmosis Membranes" in *Desalination*, 32, 127-135.

Derjaguin, B.V. and L. Landau, 1941. *Acta Physicochim.* (USSR) 14, 633-662.

Giddings, J.C., 1966. "A New Separation Concept Based on a Coupling of Concentration and Flow Nonuniformities" in Separation Science 1:123-125.

_____, 1978. "Displacement and Dispersion of Particles of Finite Size in Flow Channels with Lateral Forces – Field Flow Fractionation and Hydrodynamic Chromatography" in *Separation Science and Technology* 13:241-254.

_____, 1993. "Field Flow Fractionation: Analysis of Macromolecular, Colloidal, and Particulate Materials" in *Science* 260:1456-1465.

_____, 1997. "Factors Influencing Accuracy of Colloidal and Macromolecular Properties Measured by Field Flow Fractionation" in *Analytical Chemistry* 69:552-557.

Howe, K. and M. Clark, 2002. "Fouling of microfiltration and ultrafiltration membranes by natural waters" in *Environ. Sci Technol.*, 36, 3571-3576.

Martinez, R.L., 1999. "Will Membranes Replace Conventional Treatment?" in *Journal AWWA* 91(6): 24-32.

Martin, M., 1999. "Deviations to Classical Retention Theory of Field Flow Fractionation" in *Journal of Chromatography* A. 831:73-87.

Martin, M., and P.S. Williams, 1992. "Theoretical Basis of Field Flow Fractionation" in *NATO ASI Series C: Theoretical Advancement in Chromatography and Related Separation Techniques*, F. Dondi and G. Guiochon, Kluwer (eds), Academic Publishers.

Ranville, J.F. and R. Schmiermund, 1997. "An Overview of Environmental Colloids" in, *Perspectives in Environmental Chemistry*, D. Macalady, (ed.), Oxford University Press, Oxford, United Kingdom.

Suslov, S.A., A.J. Roberts, 1999. "Advection-dispersion in symmetric field-flow fractionation channels" in *Journal of Mathematical Chemistry* 26:27-46.

Ullmann, L., G. Amy, J.F. Ranville, and F.H. Frimmel, 2000. Development of Flow Field Flow Fractionation with UV-/DOC-detection for the characterization of Dissolved Organic Carbon, Conference on Refractory Organic Substances in the Environment-ROSE II, August 1-3, 2000, University of Karlsruhe, Germany.

Verwey, E.J., and J.Th.G. Overbeek, 1948. *Theory of the Stability of Lyophobic Colloids*, Elsevier, Amsterdam.

Williams, P.S., Y. Xu, P. Reschiglian, and J.C. Giddings, 1997. "Colloid Characterization by Sedimentation Field Flow Fractionation: Correction for Particle-Wall Interaction" in *Analytical Chemistry* 69:349-360.

Wright, S.C., 2002. Relating complex solute mixture characteristics to membrane fouling using flow field flow fractionation. PhD. Dissertation, Department of Civil, Environmental, and Architectural Engineering, University of Colorado.

Appendix

A: Moments Analysis of the RTD

The residence time distributions (RTD), both experimentally –determined and computed from the advection-dispersion model of Suslov and Roberts, can be analyzed for the moments of the distribution. The experimental RTD are obtained by monitoring detector response versus time. Differences between computed and observed moments provide information on solute-membrane and membrane-membrane interactions. A method was developed by Wright (2002) to analyze measured or computed RTD for their moments. The procedure is as follows:

Step1. The RTD baseline was adjusted to account for any detector 'drift' using the FFF analysis software (PostNovam, Salt Lake City, UT).

Step 2. Output (time vs. detector response) was imported into a Microsoft Excel spreadsheet.

Step 3. The experimental void peak time was determined from the detector response and time array using the raw data unadjusted for corrected baseline. Generally this was accomplished using a zero field RTD.

Step 4. The efflux time (beginning of peak) and end of peak were determined using the detector response array. The efflux time was taken as the time corresponding to the first value in the detector response array that showed a deviation from the baseline. The end of the peak elution was taken as the time corresponding to the stable value of the adjusted baseline of the concentration array.

Step 5. The detector response array corresponding to the sample RTD was normalized to 1.0. It is reported as $C_{(t)\ Normalized\ (Peak)}$.

Step 6. The sum of the values was determined for the $C_{(t)\ Normalized\ (Peak)}$ array.

Step 7. The probability density function of the $C_{(t)\ Normalized\ (Peak)}$ array was determined as:

$$E_{(d_p)\,NormalizedPeak} = \frac{C_{(t)\,NormalizedPeak}}{\sum C_{(t)\,NormalizedPeak}}$$

Step 8. The retention time, t_r, was determined for each data point of the $C_{(t)\ Normalized\ (Peak)}$ array by subtracting the dead time between the channel and the detector from the corresponding time array data point. The void time, t_0, was determined from the void peak (adjusted for pre-and post-channel dead time).

Step 9. The retention ratio, R, for each point of the concentration array of the RTD was determined as:

$$R = \frac{t_0}{t_r}$$

Step 10. The retention parameter, λ, was determined as:

$$\lambda = \frac{R}{6(1-R)^{1/3}}$$

Step 11. The particle diameter, d_p, for each point of the probability density function was determined as:

$$d_p = \frac{1}{\lambda} * \frac{kTV^0}{3\pi\eta V_c w^2}$$

where k is the Boltzman constant (1.38 x 10^{-23} J-K^{-1}), T is the absolute temperature (K), V^0 is the Fl-FFF void volume (cm^3), η, is the dynamic viscosity (kPa-s), V_c is the Fl-FFF channel volumetric flow rate (cm^3-s^{-1}), and w is the estimated Fl-FFF channel thickness (cm).

Step 14. The 0^{th} moment is determined to be the particle diameter at the peak maximum of the normalized RTD.

Step 15. The 1^{st} moment (mean particle diameter) for the RTD was determined as:

$$Mean = \sum_{i=efflux}^{i=end} d_{p_i} E_{(d_p)i}$$

Step 16. The 2^{nd} moment (variance) of the particle diameter for the RTD was determined as:

$$Variance = \sum_{i=efflux}^{i=end} (d_{p_i} - d_{p_{Mean}})^2 E_{(d_p)i}$$

Step 17. The 3rd moment (skew) of the particle diameter for the RTD was determined as:

$$Skew = \sum_{i=efflux}^{i=end} (d_{p_i} - d_{p_{Mean}})^3 E_{(d_p)i}$$

Step 18. The 4th moment (kurtosis) of the particle diameter for the RTD was determined as:

$$Kurtosis = \sum_{i=efflux}^{i=end} (d_{p_i} - d_{p_{Mean}})^4 E_{(d_p)i}$$